Multinanoparticle scattering in a multimode microspheroid resonator

You-Ling Chen* and Yong-Zhen Huang
State Key Laboratory on Integrated Optoelectronics, Institute of Semiconductors, Chinese Academy of Sciences, Beijing 100083, People's Republic of China

(Received 19 November 2018; published 11 February 2019)

We theoretically investigate the scattering of multiple Rayleigh nanoparticles in a microspheroid resonator which supports multiple polar whispering gallery modes. Different from a standard microsphere resonator in which polar modes with the same radial and angular mode numbers are degenerate, a spheroid resonator supports spectrally nondegenerate polar modes. The mode splitting, mode shift, and linewidth broadening of polar modes are deduced at the presence of multiple Rayleigh scatterers following the Weisskopf-Wigner semi-QED treatment. It is found that the radial, polar, and azimuthal coordinates of the nanoparticle can be inferred from the transmission spectra of the polar modes. In particular, the changes of both the mode shift and linewidth broadening show cosinoidal dependence on the azimuthal angle. Our scheme provides an efficient platform to locate the three-dimensional positions of multiple nanoparticles in a microcavity, which may push the microcavity sensing to sizing and further quantitative measurements.

DOI: 10.1103/PhysRevA.99.023818

I. INTRODUCTION

Optical whispering-gallery-mode (WGM) microcavities have drawn increasing attention due to their ultrahigh Q factors and small mode volumes. Notably, the light-matter interaction in the WGM microcavity is strongly enhanced, showing great potential in both fundamental and applied physics [1–4]. As a prominent optical device, WGM microcavity has found wide applications in the multidisciplinary fields such as cavity quantum electrodynamics [5,6], quantum optomechanics [7,8], nonlinear optics [9,10], classical and wave chaos [4,11,12], optical frequency comb [13], low-threshold microlasing [2,14,15], and ultrasensitive sensing [16–20]. Over the past few years, WGM microcavity has also witnessed many interesting phenomena, including symmetry breaking [21–24], exceptional points [25–27], and nonreciprocal light transmission [28,29].

Single nanoparticle induced scattering in a WGM microcavity has been studied intensively as it provides a basis for exploring modal coupling [30–33] and implementing nanoparticle detection [19,20,34]. The nanoparticles which appear in the evanescent field of the WGM microresonator will notably affect the mode spectra in the form of resonant frequency shift [35–40], mode splitting [34,41,42], or mode linewidth broadening [43–45]. It is also found that even a single nanoparticle can significantly modify the far-field distribution of the cavity mode [46–48]. Multiple nanoparticle induced scattering in WGM microcavities is attracting much research concern because there is more than one scatterer in most realistic physical processes [49]. For example, Zhu *et al.* have experimentally realized the controlled mode splitting using two nanofiber tips [50]. Therein, a two-scatterer model is developed in which the two standing-wave modes (SWMs) distribute themselves to obtain the maximum mode splitting. Later, Yi *et al.* have proposed a theoretical model to analyze the mode splitting induced by multiple Rayleigh scatterers [51]. The key idea is that the phase information should be considered for the clockwise (CW) and counterclockwise (CCW) traveling WGMs. Furthermore, Wiersig has found that multiparticle scattering in a microdisk is asymmetric, forming nonorthogonal copropagating modes rather than the standard SWMs [52]. This finding triggers the studies on exceptional points and their applications in ultrahigh-Q WGM microcavities [25,26].

However, all the aforementioned studies on nanoparticle scattering in WGM microcavities are performed in cavities with circular symmetry. Typically, the WGMs are labeled by three mode numbers: the radial mode number q, the angular mode number l, and the azimuthal mode number m. For given q and l, there are $2l+1$ modes with m ranging from $-l$ to l. The modes with different m are called polar modes. In a microcavity with circular symmetry such as a standard microsphere, these polar modes are degenerate and indistinguishable in the frequency domain. Nonetheless, for a slightly prolate microspheroid, this degeneracy is lifted, and a recent experiment shows the latitude angle detection of a Rayleigh scatterer through the shifts of two polar modes in a spheroidal microcavity [53]. Angular position detection of a single nanoparticle is realized through the split modes in an asymmetric rolled-up optical microcavity [54,55]. In addition, theoretical study on the frequency shift induced by a single nanoparticle in a spheroidal resonator has been proposed [56]. These experimental demonstrations and theoretical study represent an important step towards quantitative measurements by using optical microcavities.

In this paper, we propose a theoretical model to comprehensively study the multinanoparticle scattering in a microspheroid resonator which supports multiple nondegenerate polar modes. Due to the different electromagnetic field distributions, the polar modes in a microspheroid respond discriminatively to the binding of nanoparticles, which provides an

*ylchen@semi.ac.cn

 ©2019 American Physical Society

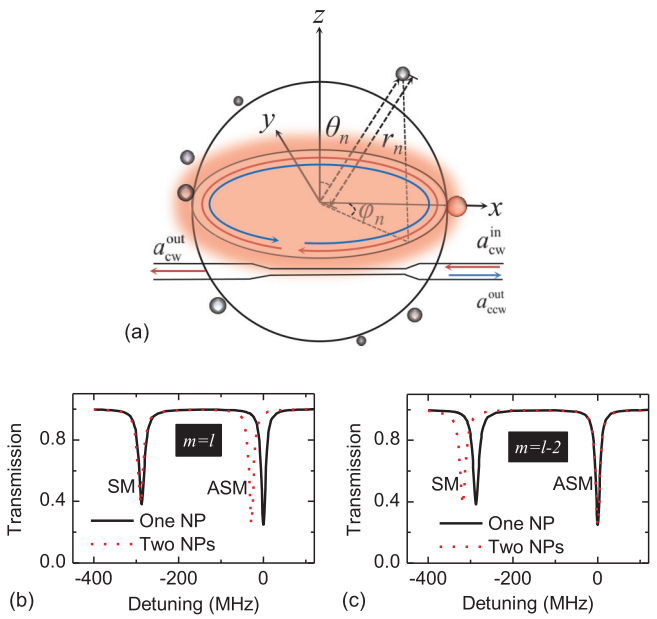

FIG. 1. (a) Schematic of the proposed system: multiple Rayleigh nanoparticles are located in the evanescent field of a slightly prolate WGM microspheroid. The microcavity is coupled by a tapered fiber. $(r_n, \theta_n, \varphi_n)$ are the radial, polar, and azimuthal positions of the nth scatterer. $a_{\mathrm{CW}}^{\mathrm{in}}$ denotes the input field of the clockwise mode, while $a_{\mathrm{CW}}^{\mathrm{out}}$ and $a_{\mathrm{CCW}}^{\mathrm{out}}$ are the output fields of the clockwise and counterclockwise modes. (b),(c) Typical transmission spectra of the polar modes with $m = l$ and $m = l - 2$ upon the attachment of one nanoparticle (black solid curve) and two nanoparticles (red dotted curve) to the microcavity. The radii of the first and second scatterers are 100 nm and 40 nm, respectively.

efficient way for implementing three-dimensional positioning as well as sizing of multiple nanoparticles. The paper is organized as follows. In Sec. II, we build a general model to analyze the scattering induced by multiple Rayleigh scatterers in a slightly prolate microspheroid. The mode splitting, mode shift, and linewidth broadening of split polar modes are achieved following the Weisskopf-Wigner semi-QED treatment. In Sec. III, we discuss the three-dimensional positioning of a single nanoparticle as well as multiple Rayleigh nanoparticles through the transmission spectra of split polar modes. The azimuthal angle can be extracted combining the shifts of three neighboring split polar modes, while the single mode is sufficient for achieving the radial position. The upper limit of the number of scatterers that can be detected through this method is calculated. In Sec. IV, sizing of nanoparticles is proposed. A summary is presented in Sec. V.

II. THEORETICAL MODEL

The interacting system is illustrated in Fig. 1(a). A slightly prolate microspheroid is evanescently coupled to a tapered fiber. Subwavelength Rayleigh nanoparticles appear in the evanescent fields of the microcavity modes. Since the cavity modes that we are concern with have the same radial mode number q and angular mode number l, it is convenient to denote them using just the polar mode number m in the following analysis. Because all the scatterers are much smaller than the wavelength, the Weisskopf-Wigner semi-QED treatment is appropriate for solving the interaction between the microcavity and multiple scatterers [30]. The microcavity supports pairs of degenerate traveling modes, i.e., the CW and CCW modes. Under dipole approximation, the electric fields of the WGMs polarize the nanoparticles. Assuming that the distances between the nanoparticles are large enough, the interaction between them can be omitted. Thus the total Hamiltonian of the system consists of three parts: the free Hamiltonian H_0 of the WGMs and the reservoir, the scattering into the same or counterpropagating cavity modes described by the Hamiltonian H_1, and the scattering into the reservoir modes described by H_2. Supposing there are $N + 1$ nanoparticles; the system Hamiltonian can be written as

$$H = H_0 + H_1 + H_2, \tag{1a}$$

$$H_0 = \sum_{m=-l}^{l} \sum_{p} \hbar\omega_m a_{m,p}^{\dagger} a_{m,p} + \sum_{j} \hbar\omega_j b_j^{\dagger} b_j, \tag{1b}$$

$$H_1 = \sum_{m=-l}^{l} \sum_{n=0}^{N} \sum_{p,p'} \hbar g_{n,m,p,p'} a_{m,p}^{\dagger} a_{m,p'}, \tag{1c}$$

$$H_2 = \sum_{m=-l}^{l} \sum_{n=0}^{N} \sum_{j,p} \hbar g_{n,m,j,p} (b_j^{\dagger} a_{m,p} + a_{m,p}^{\dagger} b_j), \tag{1d}$$

where $\hbar = h/2\pi$ is the reduced Planck constant; $a_{m,p}^{\dagger}$ ($a_{m,p'}^{\dagger}$, $b_j^{\dagger}$) and $a_{m,p}$ ($a_{m,p'}$, b_j) are the creation and annihilation operators of the (m, p) cavity mode (the m, p' cavity mode, the jth reservoir mode), with $p, p' =$ CW or CCW denoting clockwise or counterclockwise cavity modes; ω_m and ω_j represent the resonant frequencies of the m cavity mode and the jth reservoir mode, respectively. It is noted that each pair of CW and CCW cavity modes are degenerate in their resonant frequencies. The coupling coefficient $g_{n,m,p,p'}$ describes the scattering between the p and p' cavity modes due to the scattering of the nth nanoparticle and $g_{n,m,j,p}$ gives their side scattering to the jth reservoir mode, both of which can be calculated within the dipole approximation.

The quantized electric field of the m cavity mode at the position of the nth scatterer can be expressed by $\vec{E}_{n,m,\mathrm{CCW(CW)}} = f_m(\vec{r_n}) e^{\pm im\varphi_n} \sqrt{\hbar\omega_m/(2\varepsilon_0 V_m)}$, where $f_m(\vec{r_n})$ is the cavity mode function at the scatterer position $\vec{r_n}$, φ_n is the azimuthal angle of the nth scatterer, ε_0 is the electric permittivity of vacuum, and V_m is the mode volume of the m cavity mode. Different from the single scatterer case where the quantized electric field is assumed to be real, here the complex phase factors $e^{\pm im\varphi_n}$ have been included for the traveling CCW and CW modes. As a result, the coupling coefficients can be expressed by

$$g_{n,m,\mathrm{CW,CW(CCW,CCW)}} = g_{n,m} = -\frac{\alpha_n f_m^2(\vec{r_n})\omega_m}{2V_m}, \tag{2a}$$

$$g_{n,m,\mathrm{CW,CCW}} = g_{n,m} e^{2im\varphi_n}, \tag{2b}$$

$$g_{n,m,\mathrm{CCW,CW}} = g_{n,m} e^{-2im\varphi_n}, \tag{2c}$$

$$g_{n,m,j,\mathrm{CCW(CW)}} = -\frac{\alpha_n f_m^2(\vec{r_n})\omega_m}{2\sqrt{V_m V_c}} e^{\pm im\varphi_n}, \tag{2d}$$

where α_n denotes the polarizability of the nth scatterer and V_c is the mode volume of the reservoir mode. Note that Eq. (2a) gives the forward scattering coefficient, Eqs. (2b) and (2c) describe the backscattering coefficients, while Eq. (2d) represents the side scattering coefficient.

From Eqs. (1a)–(1d) and (2a)–(2d), the Heisenberg equations of motion for the system coupled to a tapered fiber can be obtained:

$$\begin{aligned}\frac{da_{m,\mathrm{CW(CCW)}}}{dt} =& -i\left(\omega_m + \sum_{n=0}^{N} z_{n,m} - i\frac{\kappa_m}{2}\right)a_{m,\mathrm{CW(CCW)}} \\ & - i\sum_{n=0}^{N} z_{n,m}e^{\pm 2im\varphi_n}a_{m,\mathrm{CCW(CW)}} \\ & - \sqrt{\kappa_{1,m}}a^{\mathrm{in}}_{m,\mathrm{CW(CCW)}},\end{aligned} \tag{3}$$

where $z_{n,m} = g_{n,m} - \frac{i}{2}\gamma_{n,m}$ with $\gamma_{n,m} = [\alpha_n^2 f_m^2(\vec{r_n})\omega_m^4]/(6\pi v^3 V_m)$ being the damping rate induced by the nth scatterer and v the speed of light in the surrounding environment, $\kappa_m = \kappa_{0,m} + \kappa_{1,m}$ with $\kappa_{0,m}$ describing the intrinsic damping rate of the m cavity mode and $\kappa_{1,m}$ denoting the coupling rate to the taper, and $a^{\mathrm{in}}_{m,\mathrm{CW(CCW)}}$ represents the CW (CCW) input field. We define a coefficient $\eta_m = \sqrt{\sum_{n=0}^{N} z_{n,m}e^{-2im\varphi_n}}/\sqrt{\sum_{n=0}^{N} z_{n,m}e^{2im\varphi_n}}$, and correspondingly two new eigenmodes of the system can be defined as $a_{m,\pm} = \pm\eta_m a_{m,\mathrm{CW}} + a_{m,\mathrm{CCW}}$. Separating the time-dependent operators $a_{m,p}$ in Eq. (3) into slowly varying parts and oscillatory parts $a_{m,p} = \tilde{a}_{m,p}e^{-i\omega t}$, we can obtain the steady-state equation

$$\left[i(-\Delta_m + g_{m,\pm}) + \frac{\kappa_m + \Gamma_{m,\pm}}{2}\right]\tilde{a}_{m,\pm} + \sqrt{\kappa_{1,m}}\tilde{a}^{\mathrm{in}}_{m,\pm} = 0, \tag{4}$$

where $\Delta_m = \omega - \omega_m$ denotes the frequency detuning between the carrier and the m mode, and $g_{m,\pm}$ and $\Gamma_{m,\pm}$ are the shifts and broadenings of the "$m,\pm$" modes compared to the originally degenerate modes, with

$$g_{m,\pm} = \mathrm{Re}\left[\sum_{n=0}^{N} z_{n,m} \pm \sqrt{\left(\sum_{n=0}^{N} z_{n,m}e^{2im\varphi_n}\right)\left(\sum_{n=0}^{N} z_{n,m}e^{-2im\varphi_n}\right)}\right], \tag{5}$$

$$\Gamma_{m,\pm} = -2\ \mathrm{Im}\left[\sum_{n=0}^{N} z_{n,m} \pm \sqrt{\left(\sum_{n=0}^{N} z_{n,m}e^{2im\varphi_n}\right)\left(\sum_{n=0}^{N} z_{n,m}e^{-2im\varphi_n}\right)}\right]. \tag{6}$$

The complex eigenfrequencies of the "$m,+$" and the "$m,-$" modes are

$$\begin{aligned}\omega_{m,\pm} =& \omega_m - \frac{i\kappa_m}{2} + \sum_{n=0}^{N} z_{n,m} \\ & \pm \sqrt{\left(\sum_{n=0}^{N} z_{n,m}e^{2im\varphi_n}\right)\left(\sum_{n=0}^{N} z_{n,m}e^{-2im\varphi_n}\right)}.\end{aligned} \tag{7}$$

From Eqs. (5)–(7), it is not difficult to find that the spectra of the multiple polar modes contain information on the three-dimensional position of the scatterers. In detail, the azimuthal angle φ_n is apparent. At the same time, $z_{n,m}$ depends on the factor $f_m^2(\vec{r_n})$ which relies on the radial position r_n and the polar angle θ_n. As a result, the three-dimensional position of the nth scatterer $(r_n, \theta_n, \varphi_n)$ could be inferred from the spectra of the multiple polar modes.

III. THREE-DIMENSIONAL POSITIONING OF NANOPARTICLES

As an important application, in this section we discuss the three-dimensional positioning of nanoparticles from the transmission spectra of multiple polar modes. Under certain conditions, the expressions of the mode shift, mode broadening, and eigenfrequencies can be simplified. For example, if the coupling induced by the first nanoparticle ($n = 0$) is much stronger than that induced by the succeeding nanoparticles, that is

$$|z_0| \gg \left|\sum_{n=1}^{N} z_n e^{\pm 2im\varphi_n}\right|, \tag{8}$$

Eqs. (5)–(7) can be further reduced through the Taylor expansion as

$$g_{m,\pm} = g_{0,m} \pm g_{0,m} + \sum_{n=1}^{N} g_{n,m}[1 \pm \cos(2m\varphi_n)], \tag{9}$$

$$\Gamma_{m,\pm} = \gamma_{0,m} \pm \gamma_{0,m} + \sum_{n=1}^{N} \gamma_{n,m}[1 \pm \cos(2m\varphi_n)], \tag{10}$$

$$\begin{aligned}\omega_{m,\pm} =& \omega_m + z_{0,m} \pm z_{0,m} + \sum_{n=1}^{N} z_{n,m}[1 \pm \cos(2m\varphi_n)] \\ & - \frac{i\kappa_m}{2} + O(|Z_{n,m}|/|z_{0,m}|).\end{aligned} \tag{11}$$

Note that the criterion Eq. (8) can routinely be satisfied by preattatching a Rayleigh scatterer which is much larger than the other scatterers to the cavity surface. In the following, we call the first scatterer which is relatively larger the "preset scatterer," while the other scatterers are called the "target scatterers."

A. Positioning of a single nanoparticle

In this subsection, for simplicity, we will first discuss the positioning of a single target scatterer. The preset scatterer

induces the original splitting. Each pair of degenerate CW and CCW modes with polar number m splits into two new modes: the "$m, +$" mode and the "$m, -$" mode. Upon the entrance of the target nanoparticle, the transmission spectrum changes accordingly. Comparing the results of one target with that of no target, the relative changes of the frequency shifts and linewidths of the $m, +$ mode and the $m, -$ mode caused by the single target scatterer are

$$\Delta g_{m,\pm} = g_{1,m}[1 \pm \cos(2m\varphi_1)], \tag{12}$$

$$\Delta \Gamma_{m,\pm} = \gamma_{1,m}[1 \pm \cos(2m\varphi_1)]. \tag{13}$$

According to Eqs. (12) and (13), the changes of spectra are discriminable for different polar modes. The radial position r_1, the azimuthal angle φ_1, as well as the polar angle θ_1 can be achieved from the transmission spectra. Polar angle detection has been experimentally realized by monitoring the ratio of shifts from two different polar modes without splitting in a spheroidal microcavity with modest quality factor [53]. In what follows, we focus our study on the azimuthal angle as well as the radial position instead.

1. Azimuthal angle

The azimuthal angle of the target nanoparticle φ_1 can be derived through the changes of the frequency shifts $\Delta g_{m,\pm}$ of the splitted neighboring $m, +$ and $m, -$ polar modes. Explicitly,

$$\cos(2m\varphi_1) = \frac{\Delta g_{m,+} - \Delta g_{m,-}}{\Delta g_{m,+} + \Delta g_{m,-}}. \tag{14}$$

Combining the trigonometric formula

$$\cos(2\varphi_1) = \frac{\cos[2(m+1)\varphi_1] + \cos[2(m-1)\varphi_1]}{2\cos(2m\varphi_1)}, \tag{15}$$

the azimuthal position of the target can be extracted correspondingly. In the above expression, the values of $\cos[2(m+1)\varphi_1]$, $\cos[2(m-1)\varphi_1]$, and $\cos(2m\varphi_1)$ can be obtained through the changes of mode shift of three adjacent polar modes $m+1$, m, and $m-1$.

The azimuthal angle detection scheme is immune to the temperature fluctuation since the factors related to temperature are canceled from the ratio of shifts in the same microspheroid. The errors induced by the transmission spectrum measurement are amplified by a factor $|1/[2\cos(2m\varphi_1)]|$ and become infinite when $\cos(2m\varphi_1) = 0$. To control the error, a nonzero term $\cos(2m\varphi_1)$ should be chosen as the denominator.

2. Radial position

While three neighboring polar modes are needed to achieve the azimuthal angle of the target nanoparticle, single mode is sufficient for deriving the radial position through four steps. First, according to Eq. (12), the coupling parameter $g_{1,m}$ can be inferred from the changes of frequency shift of the $m, +$ and $m, -$ polar modes, $g_{1,m} = (\Delta g_{m,+} + \Delta g_{m,-})/2$. Second, according to Eqs. (2a), (12), (13), and the expression of $\gamma_{n,m}$, the polarizability of the target scatterer α_1 can be achieved through the ratio of the relative changes of mode broadening to mode shift of the $m, +$ or $m, -$ polar mode

$$\alpha_1 = \frac{3\pi\nu^3}{\omega_m^3}\frac{\gamma_{1,m}}{g_{1,m}} = \frac{3\pi\nu^3}{\omega_m^3}\frac{\Delta\Gamma_{m,+(-)}}{\Delta g_{m,+(-)}}. \tag{16}$$

Third, $f_m^2(\overrightarrow{r_1})$ can be calculated through $g_{1,m}$ and α_1 according to Eq. (2). Finally, the radial position r_1 can be obtained through the expression of $f_m^2(\overrightarrow{r_1})$.

The typical evanescent field distribution $e^{-h/L}$ is used to fit the field distribution $f_m^2(\overrightarrow{r_1})$, where $h = r_1 - R$ is the distance from the center of the target nanoparticle to the cavity surface, R is the radius of the WGM cavity, and L is the characteristic evanescent length which needs to be calculated. According to Refs. [57,58], $kR = l(n_e/n_c)[1 + \alpha_q 2^{-1/3} l^{-2/3} + O(l^{-1})]$, with n_e and n_c being the refractive indices of the surrounding environment and the cavity and α_q being the qth root of the Airy function with q denoting the radial mode number. At the same time, the characteristic evanescent length $L \simeq 1/[k\sqrt{(n_c/n_e)^2 - 1}]$. After some derivation, the radial position of the target nanoparticle can be expressed by

$$r_1 = R + \frac{Rn_c}{\sqrt{n_c^2 - n_e^2}(l + \alpha_q 2^{-1/3} l^{1/3})} \times \ln\left|\frac{3\pi\nu^3}{\omega_m^2 V_m}\frac{\Delta\Gamma_{m,+}}{\Delta g_{m,+}(\Delta g_{m,+} + \Delta g_{m,-})}\right|. \tag{17}$$

Through Eq. (17), we can find that one single polar mode with mode numbers (q, l, m) is adequate for the detection of the radial position r_1 combining the changes of linewidth and mode shifts.

B. Positioning of multiple nanoparticles

In most realistic sensing applications there is more than one scatterer. The exact expressions of the eigenfrequencies, the shifts of resonance frequencies, and the broadenings of the $m, +$ and $m, -$ modes have been derived in Sec. II. As long as the coupling induced by the preset scatterer is much stronger than that induced by the succeeding scatterers, the effect of higher-order term $O(|Z_{n,m}|/|z_{0,m}|)$ can be neglected. Three-dimensional positioning of multiple target scatterers can be implemented at the presence of a relatively larger preset scatterer. Explicitly, the position information of the first target scatterer can be obtained by comparing the spectra before and after the attachment of it. Similarly, the position of the succeeding N target nanoparticles can be achieved following this method.

In the following, we will discuss the upper limit of the number of nanoparticles that can be detected through this method. Figure 2(a) shows the transmission spectra under different numbers of target nanoparticles $N = 10$, 50, 100, and 200, and the Q factor of the cavity mode is assumed to be $Q = 1 \times 10^8$. The nanoparticles are assumed to be spheres with refractive index 1.50, and the surrounding medium is supposed to be air. It is found that, as long as Q is very high, the mode splitting can easily be resolved. This is because the original linewidth ω_m/Q is much smaller than the splitting. At the same time we can find that the mode splitting changes randomly with the increase of N. For example, the splitting for $N = 100$ is obviously smaller than that for $N = 50$, while the splitting for $N = 200$ is apparently larger than that for

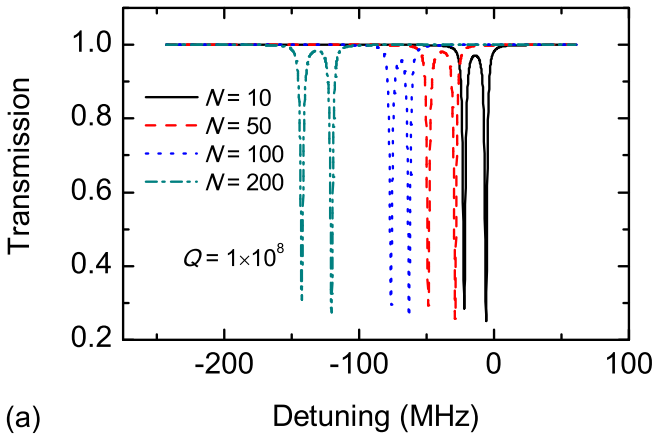

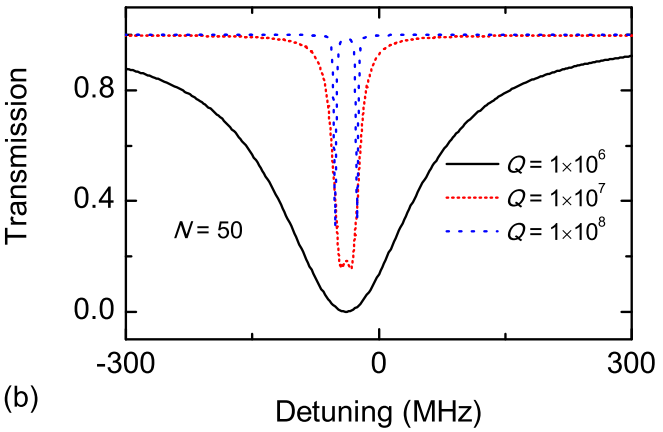

FIG. 2. (a) Transmission spectra under different numbers of target nanoparticles $N = 10$, 50, 100, and 200. The quality factor of the m cavity mode $Q = 1 \times 10^8$. (b) Typical transmission spectra under different values of Q. N is assumed to be 50, $\lambda = 1550$ nm, and $f_m^2(\vec{r_n}) = 0.2$. Radii of the cavity, the preset nanoparticle, and target nanoparticles are $R = 50$ μm, $r_0 = 70$ nm, and $r_n = 30$ nm.

$N = 100$. The reason behind this is the random binding position of the target nanoparticles. Figure 2(b) shows the influence of mode Q factor on the transmission spectrum. N is assumed to be 50. For a low Q mode, for example, $Q = 1 \times 10^6$, the mode splitting cannot be resolved. When Q increases to 1×10^7, the $\pm$ modes become resolvable. For a high Q mode with $Q = 1 \times 10^8$, the splitting is quite apparent.

It is well known that the mode splitting of the "+" and "−" modes can be resolved only if the splitting exceeds the average of the resonant linewidth, which is composed by two parts: the original linewidth and the broadening $\Gamma_{m,\pm}$. For simplicity, we focus our discussion on the case of N identical target scatterers with the same value of $g_{n,m}$ and $\gamma_{n,m}$ at the presence of a much larger preset scatterer. The splitting between the $m,+$ and $m,-$ modes and the linewidth broadenings can be achieved through Eqs. (9) and (10). The criterion can be expressed by

$$2\left|g_{0,m} + g_{n,m}\sum_{n=1}^{N}\cos(2m\varphi_n)\right| > \frac{\omega_m}{Q} + \gamma_{0,m} + N\gamma_{n,m}. \quad (18)$$

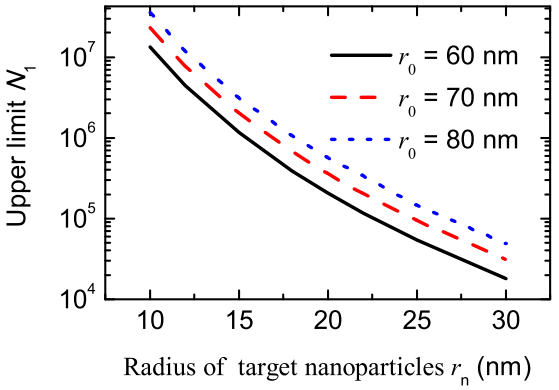

FIG. 3. Upper limit N_1 of the number of target scatterers that can be resolved through mode splitting under different values of radii for target scatterer r_n between the range of 10 nm to 30 nm. The radius of the preset scatterer is set at $r_0 = 60$ nm, $r_0 = 70$ nm, and $r_0 = 80$ nm for the black solid curve, the red dashed curve, and the blue dotted curve. Quality factor of the cavity mode $Q = 1 \times 10^8$, $\lambda = 1550$ nm, and cavity radius $R = 50$ μm.

Figure 3 shows the upper limit N_1 under different values of radii for the preset and target nanoparticles calculated from Eq. (18). The larger the preset scatterer is and the smaller the target scatterers are, the more nanoparticles can be detected. From Fig. 3 we can find that the mode splitting can be well resolved for a very large number of target nanoparticles. However, more consideration should be given to the upper limit of the number of target nanoparticles which can be detected. If too many scatterers bind onto the cavity, the coupling strength condition will be broken. For example, if the target scatterers are located on the equator randomly, the term $|\sum_{n=1}^{N} e^{\pm 2im\varphi_n}|$ in Eq. (8) will be proportional to $\sqrt{N}$ as N grows [51]. If we set the criteria of the coupling strength condition as $|Z_{n,m}| = |\sum_{n=1}^{N} z_{n,m}e^{\pm 2im\varphi_n}| \leqslant |z_{0,m}|/10$, the upper limit can be expressed as $N_2 = |z_{0,m}/Z_{n,m}|^2/100$. Figure 4 shows the upper limit N_2 under different values of r_n and r_0. From Fig. 4 we can find that N_2 decreases rapidly with the radius of the target nanoparticle. Take the black solid curve of $r_0 = 60$ nm as an example: when $r_n = 10$ nm which

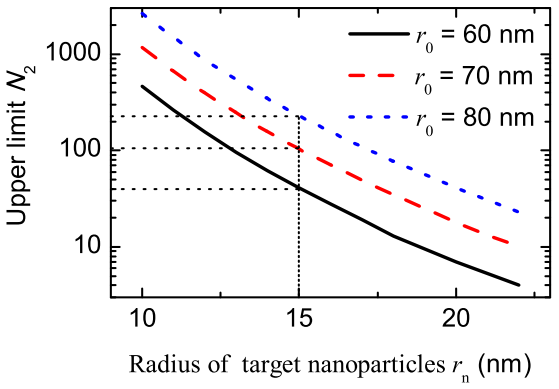

FIG. 4. Upper limit N_2 of the number of target nanoparticles that can guarantee the coupling strength condition under different radii of the target scatters r_n and preset scatterer r_0. Other parameters are the same as in Fig. 3.

equals $r_0/6$, N_2 can be as large as 466; when $r_n = 20\,\text{nm}$ which equals $r_0/3$, N_2 decreases severely to 7. For the typical value of $r_n = 15$ nm, N_2 is around 40, 100, and 230 for the cases of $r_0 = 60$ nm, $r_0 = 70$ nm, and $r_0 = 80$ nm. It is not difficult to understand that N_2 rather than N_1 is the upper limit of the detectable number of target nanoparticles for our scheme.

IV. SIZING OF NANOPARTICLES

In our system, sizing of nanoparticles can routinely been realized. According to Eq. (16), the polarizability α_1 can be obtained combining the shift and broadening signals of one polar mode. It should be noticed that our scheme is different from Ref. [34] or Ref. [53]. Here we propose to use the ratio of the relative changes of mode broadening to mode shift either of the splitted $m, +$ mode $\Delta\Gamma_{m,+}/\Delta g_{m,+}$ or $m, -$ mode $\Delta\Gamma_{m,-}/\Delta g_{m,-}$, rather than the splitting between the $+$ and $-$ modes [34]. In Ref. [53], sizing of nanoparticles is based on the mode shift in a microcavity with modest quality factor in which no mode splitting can be observed. For a spherical Rayleigh nanoparticle, the radius a can be expressed by

$$a = \frac{v}{\omega_m}\left[\frac{3\left(n_t^2 + 2n_e^2\right)\Delta\Gamma_{m,+}}{4\left(n_t^2 - n_e^2\right)\Delta g_{m,+}}\right]^{1/3}, \tag{19}$$

where n_t is the refractive index of the target nanoparticle. From Eq. (19) it is easy to find out that the broadening and shift information of one splitted polar mode $m, +$ is sufficient for the accurate sizing of a spherical Rayleigh nanoparticle. Whereas in Ref. [53], besides the mode shift of one polar mode, the knowledge of the latitude angle is the prerequisite for nanoparticle sizing.

V. CONCLUSION

In summary, we have proposed a theoretical model to analyze the scattering induced by multiple Rayleigh nanoparticles in a microspheroid which supports multiple polar modes. Due to the distinct electromagnetic field distributions, the reaction of polar modes are distinguishable upon the binding of scatterers. The mode splitting, mode shift, and linewidth broadening of split polar modes are achieved analytically. As an important application, three-dimensional positioning and sizing of multiple Rayleigh nanoparticles can be realized through the spectra change of different polar modes. After the binding of the first nanoparticle, each pair of degenerate CW and CCW modes with polar number m splits into two new modes: the $m, +$ mode and the $m, -$ mode. The azimuthal angle can be obtained comparing the shifts of three neighboring polar modes before and after the entrance of the target scatterer: the "$m, \pm$" mode, the "$m+1, \pm$" mode, and the "$m-1, \pm$" mode. The radial position of the scatterer can be extracted combining both the mode shifts and mode broadenings of the splitted $m, +$ and $m, -$ polar mode. Moreover, sizing of nanoparticles can be implemented just through the ratio of change of mode broadening to mode shift of one splitted polar mode $m, +$ or $m, -$. This mechanism can be applied not only in positioning and sizing of single nanoparticles but also of multiple Rayleigh scatterers with the number up to 40 under typical values of parameters.

ACKNOWLEDGMENTS

The authors acknowledge Prof. Y.-F. Xiao at Peking University for fruitful discussions. This work was supported by National Natural Science Foundation of China under Grants No. 11704375 and No. 61527823.

[1] K. J. Vahala, Nature (London) **424**, 839 (2003).
[2] J. Ward and O. Benson, Laser Photon. Rev. **5**, 553 (2011).
[3] J. Wang, T. Zhan, G. Huang, P. K. Chu, and Y. Mei, Laser Photon. Rev. **8**, 521 (2014).
[4] H. Cao and J. Wiersig, Rev. Mod. Phys. **87**, 61 (2015).
[5] T. Aoki, B. Dayan, E. Wilcut, W. P. Bowen, A. S. Parkins, T. J. Kippenberg, K. J. Vahala, and H. J. Kimble, Nature (London) **443**, 671 (2006).
[6] Y.-S. Park, A. K. Cook, and H. Wang, Nano Lett. **6**, 2075 (2006).
[7] T. J. Kippenberg and K. J. Vahala, Science **321**, 1172 (2008).
[8] M. Aspelmeyer, T. J. Kippenberg, and F. Marquardt, Rev. Mod. Phys. **86**, 1391 (2014).
[9] V. S. Ilchenko, A. A. Savchenkov, A. B. Matsko, and L. Maleki, Phys. Rev. Lett. **92**, 043903 (2004).
[10] D. V. Strekalov, C. Marquardt, A. B. Matsko, H. G. L. Schwefel, and G. Leuchs, J. Opt. **18**, 123002 (2016).
[11] X.-F. Jiang, C.-L. Zou, L. Wang, Q. Gong, and Y.-F. Xiao, Laser Photon. Rev. **10**, 40 (2016).
[12] X.-F. Jiang, L. Shao, S.-X. Zhang, X. Yi, J. Wiersig, L. Wang, Q. Gong, M. Lončar, L. Yang, and Y.-F. Xiao, Science **358**, 344 (2017).
[13] P. Del'Haye, A. Schliesser, O. Arcizet, T. Wilken, R. Holzwarth, and T. Kippenberg, Nature (London) **450**, 1214 (2007).
[14] X. M. Lv, Y. Z. Huang, L. X. Zou, H. Long, and Y. Du, Laser Photon. Rev. **7**, 818 (2013).
[15] L. He, S. K. Özdemir, and L. Yang, Laser Photon. Rev. **7**, 60 (2013).
[16] X. Fan, I. M. White, S. I. Shopova, H. Zhu, J. D. Suter, and Y. Sun, Anal. Chim. Acta **620**, 8 (2008).
[17] F. Vollmer and S. Arnold, Nat. Meth. **5**, 591 (2008).
[18] F. Vollmer and L. Yang, Nanophotonics **1**, 267 (2012).
[19] M. R. Foreman, J. D. Swaim, and F. Vollmer, Adv. Opt. Photon. **7**, 168 (2015).
[20] Y. Zhi, X.-C. Yu, Q. Gong, L. Yang, and Y.-F. Xiao, Adv. Mater. **29**, 1604920 (2017).
[21] L. Chang, X. Jiang, S. Hua, C. Yang, J. Wen, L. Jiang, G. Li, G. Wang, and M. Xiao, Nat. Photon. **8**, 524 (2014).
[22] B. Peng, S. K. Özdemir, F. Lei, F. Monifi, M. Gianfreda, G. L. Long, S. Fan, F. Nori, C. M. Bender, and L. Yang, Nat. Phys. **10**, 394 (2014).
[23] Q.-T. Cao, H. Wang, C.-H. Dong, H. Jing, R.-S. Liu, X. Chen, L. Ge, Q. Gong, and Y.-F. Xiao, Phys. Rev. Lett. **118**, 033901 (2017).

[24] L. Del Bino, J. M. Silver, S. L. Stebbings, and P. Del'Haye, Sci. Rep. **7**, 43142 (2017).
[25] J. Wiersig, Phys. Rev. Lett. **112**, 203901 (2014).
[26] W. Chen, S. Ozdemir, G. Zhao, J. Wiersig, and L. Yang, Nature (London) **548**, 192 (2017).
[27] Y.-K. Lu, P. Peng, Q.-T. Cao, D. Xu, J. Wiersig, Q. Gong, and Y.-F. Xiao, Sci. Bull. **63**, 1096 (2018).
[28] J. Kim, M. C. Kuzyk, K. Han, H. Wang, and G. Bahl, Nat. Phys. **11**, 275 (2015).
[29] Z. Shen, Y.-L. Zhang, Y. Chen, C.-L. Zou, Y.-F. Xiao, X.-B. Zou, F.-W. Sun, G.-C. Guo, and C.-H. Dong, Nat. Photon. **10**, 657 (2016).
[30] A. Mazzei, S. Götzinger, L. de S. Menezes, G. Zumofen, O. Benson, and V. Sandoghdar, Phys. Rev. Lett. **99**, 173603 (2007).
[31] M. L. Gorodetsky and A. D. Pryamikov, J. Opt. Soc. Am. B **17**, 1051 (2000).
[32] Y. Xu, S.-J. Tang, X.-C. Yu, Y.-L. Chen, D. Yang, Q. Gong, and Y.-F. Xiao, Phys. Rev. A **97**, 063828 (2018).
[33] J. T. Rubin and L. Deych, Phys. Rev. A **81**, 053827 (2010).
[34] J. Zhu, S. K. Özdemir, Y.-F. Xiao, L. Li, L. He, D.-R. Chen, and L. Yang, Nat. Photon. **4**, 122 (2010).
[35] S. Arnold, M. Khoshsima, I. Teraoka, S. Holler, and F. Vollmer, Opt. Lett. **28**, 272 (2003).
[36] F. Vollmer, S. Arnold, and D. Keng, Proc. Natl. Acad. Sci. USA **105**, 20701 (2008).
[37] H. Li, Y. Guo, Y. Sun, K. Reddy, and X. Fan, Opt. Express **18**, 25081 (2010).
[38] T. Lu, H. Lee, T. Chen, S. Herchak, J.-H. Kim, S. E. Fraser, R. C. Flagan, and K. Vahala, Proc. Natl. Acad. Sci. USA **108**, 5976 (2011).
[39] J. D. Swaim, J. Knittel, and W. P. Bowen, Appl. Phys. Lett. **102**, 183106 (2013).
[40] W. Yu, W. C. Jiang, Q. Lin, and T. Lu, Nat. Commun. **7**, 12311 (2016).
[41] Ş. K. Özdemir, J. Zhu, X. Yang, B. Peng, H. Yilmaz, L. He, F. Monifi, S. H. Huang, G. L. Long, and L. Yang, Proc. Natl. Acad. Sci. USA **111**, E3836 (2014).
[42] B.-B. Li, W. R. Clements, X.-C. Yu, K. Shi, Q. Gong, and Y.-F. Xiao, Proc. Natl. Acad. Sci. USA **111**, 14657 (2014).
[43] L. Shao, X.-F. Jiang, X.-C. Yu, B.-B. Li, W. R. Clements, F. Vollmer, W. Wang, Y.-F. Xiao, and Q. Gong, Adv. Mater. **25**, 5616 (2013).
[44] Y. Hu, L. Shao, S. Arnold, Y.-C. Liu, C.-Y. Ma, and Y.-F. Xiao, Phys. Rev. A **90**, 043847 (2014).
[45] M. D. Baaske, M. R. Foreman, and F. Vollmer, Nat. Nanotechnol. **9**, 933 (2014).
[46] Y.-C. Liu, Y.-F. Xiao, X.-F. Jiang, B.-B. Li, Y. Li, and Q. Gong, Phys. Rev. A **85**, 013843 (2012).
[47] N. Zhang, Z. Gu, S. Liu, Y. Wang, S. Wang, Z. Duan, W. Sun, Y.-F. Xiao, S. Xiao, and Q. Song, Optica **4**, 1151 (2017).
[48] F. Shu, X. Jiang, G. Zhao, and L. Yang, Nanophotonics **7**, 1455 (2018).
[49] Q. Li, A. A. Eftekhar, Z. Xia, and A. Adibi, Phys. Rev. A **88**, 033816 (2013).
[50] J. Zhu, S. K. Özdemir, L. He, and L. Yang, Opt. Express **18**, 23535 (2010).
[51] X. Yi, Y.-F. Xiao, Y.-C. Liu, B.-B. Li, Y.-L. Chen, Y. Li, and Q. Gong, Phys. Rev. A **83**, 023803 (2011).
[52] J. Wiersig, Phys. Rev. A **84**, 063828 (2011).
[53] D. Keng, X. Tan, and S. Arnold, Appl. Phys. Lett. **105**, 071105 (2014).
[54] S. Li, L. Ma, S. Böttner, Y. Mei, M. R. Jorgensen, S. Kiravittaya, and O. G. Schmidt, Phys. Rev. A **88**, 033833 (2013).
[55] S. Bötner, S. Li, M. R. Jorgensen, and O. G. Schmidt, Appl. Phys. Lett. **105**, 121106 (2014).
[56] L. Deych and V. Shuvayev, Phys. Rev. A **92**, 013842 (2015).
[57] A. B. Matsko and V. S. Ilchenko, IEEE J. Sel. Top. Quantum **12**, 3 (2006).
[58] C. C. Lam, P. T. Leung, and K. Young, J. Opt. Soc. Am. B **9**, 1585 (1992).